ACS APPLIED MATERIALS & INTERFACES

RESEARCH ARTICLE

www.acsami.org

Near Unity Photon-to-Electron Conversion Efficiency of Photoelectrochemical Cells Built on Cationic Water-Soluble Porphyrins Electrostatically Decorated onto Thin-Film Nanocrystalline SnO_2 Surface

Navaneetha K. Subbaiyan, Eranda Maligaspe, and Francis D'Souza*

Department of Chemistry, Wichita State University, Wichita, Kansas 67260-0051, United States

Supporting Information

ABSTRACT: Thin transparent SnO_2 films have been surface modified with cationic water-soluble porphyrins for photoelectrochemical investigations. Free-base and zinc(II) derivatives of three types of cationic water-soluble porphyrins, (P)M, viz., tetrakis(N-methylpyridyl)porphyrin chloride, (TMPyP)M, tetrakis(trimethylanilinium)porphyrin chloride, (TAP)M, and tetrakis(4′-N-methylimidazolyl-phenyl)porphyrin iodide, (TMIP)M, (M = 2H or Zn) are employed. The negative surface charge and the porous structure of SnO_2 facilitated binding of positively charged porphyrins via electrostatic interactions, in addition to strong electronic interactions in the case of (TMPyP)M binding to nanocrystalline SnO_2. The SnO_2—porphyrin binding in solution was probed by absorption spectroscopy which yielded apparent binding constants in the range of $1.5-2.6 \times 10^4$ M^{-1}. Both steady-state and time-resolved fluorescence studies revealed quenching of porphyrin emission upon binding to SnO_2 in water suggesting electron injection from singlet excited porphyrin to SnO_2 conduction band. Addition of $LiClO_4$ weakened the ion-paired porphyrin—SnO_2 binding as revealed by reversible emission changes. Over 80% of the quenched fluorescence was recovered in the case of (TMPyP)M and (TAP)M compounds but not for (TMIP)M suggesting stronger binding of the latter to SnO_2 surface. Photoelectrochemical studies performed on FTO/SnO_2/(P)M electrodes revealed incident photon-to-current conversion efficiencies (IPCE) up to 91% at the peak maxima for the SnO_2-dye modified electrodes, with very good on—off switchability. The high IPCE values have been attributed to the strong electrostatic and electronic interactions between the dye, (TMPyP)M and SnO_2 nanoparticles that would facilitate better charge injection from the excited porphyrin to the conduction band of the semiconductor. Electrochemical impedance spectral measurements of electron recombination resistance calculations were supportive of this assignment.

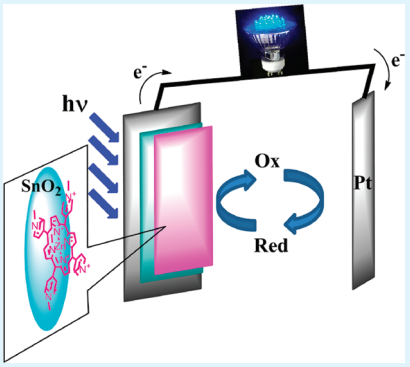

KEYWORDS: cationic porphyrins, IPCE, thin-film SnO_2, ion-pairing, solar cell

1. INTRODUCTION

Dye-sensitized solar cells (DSSCs)[1−3] have long been regarded as a promising alternative to conventional solid-state semiconductor solar cells, on the basis of their relatively high efficiency at a competitively low cost.[4−17] A considerable number of inorganic/organic structures have been designed, synthesized, and studied as molecular sensitizers[18−20] with a combination of various bandgap semiconductor nanoporous materials .[21] DSSCs based on Ru-complex dyes chemisorbed onto mesoporous titania with the help of carboxylate functionalities are shown to produce a photoelectric conversion yield of 11% under standard AM 1.5 light irradiation conditions.[1−3] Lately, organic DSSCs have received more attention because of their ease of synthesis, high molar extinction coefficient, and low cost in comparison to Ru-complexes.[19,20] Additionally, by modifying the macrocycle periphery of the dye molecules it is possible to derive mechanisms for easy immobilization of the sensitizer molecules on nanocrystalline surface.

In recent years, researchers are also looking into replacing the commonly employed mesoporous TiO_2 with other semiconducting materials.[21] Among the possibilities, nanocrystalline SnO_2 semiconductor is an attractive candidate as it possesses the conduction band lower by ~0.4 V than TiO_2, facilitating relatively efficient charge injection from the photoexcited dye molecule to semiconductor;[22] although lower open-circuit voltage (V_{OC}) could be expected due to the low lying conduction band.[23,32] In this regard, some efforts to improve the V_{OC} of SnO_2-based photoelectrochemical cells by surface treatment of MgO, ZnO, $TiCl_4$ and several insulator oxides have been explored.[24]

Exploitation of the surface properties of nanocrystalline materials to immobilize appropriately functionalized photosensitizers in a self-assembled supramolecular approach is a relatively easy yet an elegant and versatile approach.[25] Here, we report self-assembling cationic water-soluble porphyrins onto thin-film nanocrystalline SnO_2 surface via electrostatic interactions, and photoelectrochemical studies to evaluate their photon-to-current conversion efficiencies. The nanocrystalline SnO_2 colloidal particles

Received: March 6, 2011
Accepted: May 30, 2011
Published: May 30, 2011

with negatively charged surface used in the present study have a particle diameter in the range of 30−50 Å.[22] Free-base and zinc(II) derivatives of three types of water-soluble cationic porphyrins in which the positive charges progressively move far from the porphyrin π-ring (Scheme 1) have been used to decorate the SnO_2 surface. The binding of cationic porphyrins onto the SnO_2 surface were investigated by optical absorption studies while the excited state events from the singlet excited porphyrin was monitored using both steady-state and time-resolved emission techniques. The reversibility of electrostatic binding of (P)M to SnO_2 was established by varying ionic strength of the solution. Finally, photoelectrochemical studies were performed to evaluate $I-V$ characteristics and incident photon-to-current conversion (IPCE) efficiencies. As demonstrated here, the DSSC built using FTO/SnO_2/cation porphyrin electrodes with I^-/I_3^- redox mediator in acetonitrile showed very high IPCE values, in some cases, as high as 91%. Electrochemical impedance studies revealed decrease in recombination resistance under illumination due to increased local concentration of I_3^- ions near to the dye electrode−electrolyte interface as a result of regeneration of dye molecule.

2. EXPERIMENTAL METHODS

Chemicals. The free-base and zinc(II) derivatives of tetrakis(N-methyl pyridyl)porphyrin chloride, (TMPyP)M, and tetrakis(trimethylanilinium)porphyrin chloride, (TAP)M were procured from Frontier Scientific, Inc. (Logan UT) and used as received. The synthesis of tetrakis(4′-N-methylimidazolyl-phenyl)porphyrin iodide, (TMIP)H_2 is given below. Millipore water was used in all of the experiments.

5,10,15,20-Tetrakis(4′-imidazolyl-phenyl)porphyrin, (1). To a 200 mL of propionic acid, 5.8 mmol (1.0 g) of 4-(1*H*-imidazol-1-yl)benzaldehyde and 5.8 mmol of pyrrole (452 mL) were added. The solution was refluxed for 6 h and the solvent was removed under reduced pressure. The crude was purified on a basic alumina column chromatography with $CHCl_3$/MeOH (92:8 v/v) as eluent. ^{1}H NMR (400 MHz, $CDCl_3$) (in ppm): δ 8.82 (br s, 8H, β pyrrole), 8.28 (d, 8H, phenyl *H*) 8.16 (s, 4H, imidazole *H*), 7.78 (d, 8H, phenyl *H*), 7.58 (s, 4H, imidazole *H*), 7.25 (s, 4H, imidazole *H*). Mass (APCI mode in CH_2Cl_2): calcd, 879.5; found, 880.4.

5,10,15,20-Tetrakis(4′-*N*-methylimidazolyl-phenyl)porphyrin Iodide, (TMIP)H_2. Compound **1** (0.025 mmol) was treated with CH_3I (2.50 mmol) in THF (4 mL), and reaction mixture was refluxed for 3 days. The solvent was removed, and the residue was recrystallized (CH_3OH/acetone). The obtained purple solid was gel chromatographed on a Sephadex LH-60 using CH_3OH as the eluent to give a purple product. ^{1}H NMR (400 MHz, MeOD) (in ppm): δ 8.95 (br s, 8H, β pyrrole), 8.28 (d, 8H, phenyl *H*) 8.18 (s, 4H, imidazole *H*), 7.82 (d, 8H, phenyl *H*), 7.75 (s, 4H, imidazole *H*), −7.21 (s, 4H, imidazole *H*), 3.45 (s, 12H, $-CH_3$).

Preparation of Nanocrystalline SnO_2 Electrodes. These were prepared according to the literature procedure by Kamat and coworkers[22d] with few changes. A 10 μL of SnO_2 colloidal solution (Alfa Aesar, 15%) was dissolved in 10 mL of ethanol; a 500 μL of NH_4OH was added to this solution for stability. About 2 mL of colloidal solution placed on optically transparent electrode, fluorine doped indium tin oxide (FTO) (Pilkington TEC-8, 6−9 Ω/square) and dried in air on a warm plate. The electrodes were annealed in an oven for an hour in air at 673 K. The thickness of the electrode profiled using MicroXAM-3D surface profiler was around 5 ± 2 μm (see Figure S10 in the Supporting Information).

Instrumentation. Absorption spectral measurements were carried out with a Shimadzu UV2550 UV−vis spectrophotometer. The steady-state fluorescence emission was monitored by using a Cary Eclipse spectrofluorometer. Lifetime and solid state fluorescence emission were recorded using Horiba Jobin Yvon Nanolog UV−visible NIR spectrofluorometer with Time Correlated Single Photon Counting (TCSPC) lifetime option with nano-LED excitation sources (excitation pulse width ∼100−200 ps). The ^{1}H NMR studies were carried out on a Varian 400 MHz spectrometer. Tetramethylsilane (TMS) was used as an internal standard.

Scheme 1. Structures of the Cationic Water-Soluble Porphyrins Employed to Surface Modify Nanocrystalline SnO_2 for Photoelectrochemical Studies in the Present Study

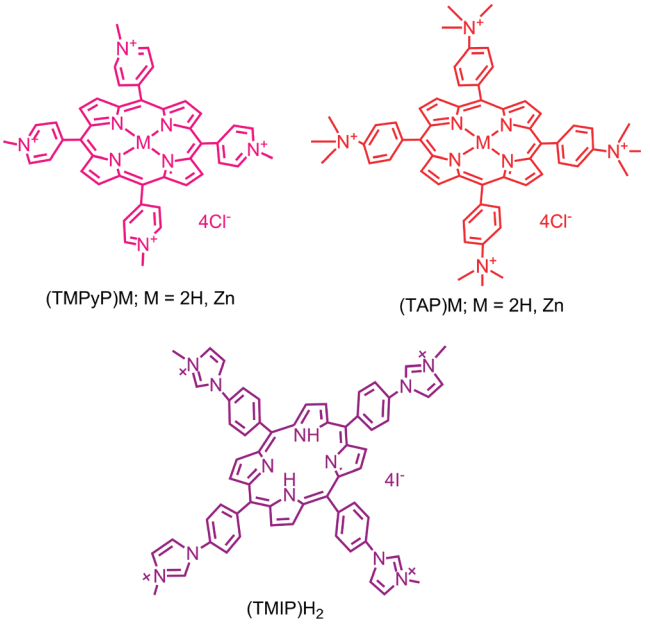

Photoelectrochemical experiments were performed in a two-electrode configuration using porphyrin adsorbed FTO/SnO_2 electrode and a platinum foil as a counter electrode. The 2 electrodes are separated using 0.7 cm Teflon spacer. A mixture of (TBA)I/I_2 in acetonitrile was used as redox mediator. The photocurrent-photovoltage ($I-V$) characteristics of the solar cells were measured using a Model 2400 Current/Voltage Source Meter of Keithley Instruments, Inc. (Cleveland, OH) under illumination with an AM 1.5 simulated light source using a model 9600 of 150 W Solar Simulator of Newport Corp. (Irvine, CA). A 340-nm filter was introduced in the light path to eliminate UV radiation. The light intensity was monitored by using an Optical Model 1916-C Power Meter of Newport. Incident photon-to-current efficiency (IPCE) measurements were performed under ∼2.5 mW cm^2 monochromatic light illumination conditions using a setup comprised of a 150 W Xe lamp with a Cornerstone 260 monochromator (Newport Corp., Irvine, CA).

Electrochemical impedance measurements were performed using EG&G PARSTAT 2273 potentiostat. Impedance data were recorded under forward bias condition from 100 kHz to 100 mHz with an A.C amplitude of 10 mV. Data were recorded under dark and A.M 1.5 illumination conditions applying corresponding V_{oc} for each electrode. The data were analyzed using ZSimpwin software from Princeton Applied Research.

3. RESULTS AND DISCUSSION

Binding of Cationic Water-Soluble Porphyrins to Nanocrystalline SnO_2. Porphyrins, (TMPyP)M and (TAP)M (M = 2H or Zn(II)), used in the present study were procured from commercial sources while (TMIP)H_2 was newly synthesized.

The optical absorption spectra of the investigated porphyrins in water is shown in Figure S1 in the Supporting Information. The free-base porphyrin derivatives revealed the anticipated intense Soret and four visible (Q) bands, whereas for the corresponding zinc derivatives, only two visible bands in addition to the intense Soret were observed because of the increased symmetry upon metal ion insertion into the ring cavity (Table 1). The peak maxima of (TMPyP)M derivatives revealed a red shift of up to 6 nm compared to the peak maxima of (TAP)M and (TMIP)M derivative. Additionally, the full width at half maxima (fwhm) values for the former derivatives was found to be over 3 times as much as that of the latter derivatives, that is, substantial broadening of the absorption peaks were observed for the (TMPyP)M derivatives. The red shift accompanied by broadening of absorption bands for (TMPyP)M derivatives has earlier been ascribed to aggregate formation with substantial interaction between the porphyrin ring π-system with peripheral positive charges.[26] On the basis of the spectral features of (TAP)M and (TMIP)M derivatives, one could conclude the presence of little or absence of aggregation and interactions with the peripheral positive charges. This may primarily due to unfavorable geometry and distant location of the positive charges from the macrocycle π-system.

As mentioned earlier, the diameter of the SnO_2 nanocrystalline colloidal particles used here are in the range of 30−50 Å suggesting their ability to accommodate one or more relatively large photosensitizer porphyrin molecules on the surface. Figure 1a shows spectral changes observed during increased addition of SnO_2 colloidal to a solution of $(TMPyP)H_2$ in water. Similar spectral changes were observed for the investigated free-base and zinc porphyrin derivatives (see Figures S1−S5 in the Supporting Information). The absorbance of SnO_2 was seen at wavelength less than 300 nm. Addition of SnO_2 caused diminished intensity of both the Soret and the visible bands. As shown in Figure 1b formation of interaction between porphyrin and SnO_2 was accompanied by a red shift of 22−26 nm for the TMPyP derivatives, and 12−17 nm for the TAP and TMIP derivatives, respectively. Earlier, the large red-shift and broadening of TMPyP upon adsorption on laponite surface (negatively charged polyionic platelets) was attributed to the flattening of the porphyrin macrocycle because of pyridyl torsion.[27] Such a structural change is also expected for (TMPyP)M binding to SnO_2 particles. Additionally, 2−4 isosbestic points were observed, indicating the existence of one equilibrium process in solution.

Table 1. Spectral Peak Position and Apparent Association Constant, K_a and Free-Energy Change for Charge Injection of Water-Soluble, Cation Porphyrins Binding to SnO_2 Nanocrystalline Particles in Water

M(P)	peak position	K_a, M^{-1}	ΔG°_{inj}, eV
(TMPyP)Zn	435, 563, 609	1.8×10^4	−0.77
(TAP)Zn	419, 554, 594	1.95×10^4	−0.93
$(TMPyP)H_2$	422, 518, 555, 584, 641	1.5×10^4	−0.44
$(TAP)H_2$	411, 513, 549, 579, 633	1.77×10^4	−0.56
$(TMIP)H_2$	414, 514, 551, 579, 634	2.6×10^4	−0.54

Figure 1b shows the difference in the absorption spectra of the SnO_2:$(TMPyP)H_2$ complex. Here, a quartz cuvette with aqueous suspension of SnO_2 in the sample beam and another cuvette with pure water in the reference beam were introduced in a dual beam spectrophotometer. Same amounts of $(TMPyP)H_2$ of known increments were added into both cuvettes and the spectrum was recorded. With increasing additions of $(TMPyP)H_2$, increasing amounts of SnO_2:$(TMPyP)H_2$ complex formation were observed as revealed by the absorption peak at 441 nm that was accompanied by depletion of the absorption of $(TMPyP)H_2$ at 422 nm band. A plot of change in absorbance δA at 441 nm vs amount of $(TMPyP)H_2$ added was linear (Figure 1b inset) suggesting that porphyrin present in solution adsorbs on SnO_2 as monomeric species. Such linear dependence was observed for all of the investigated porphyrin derivatives (see Figures S2−S5 in the Supporting Information) suggesting monomeric porphyrin adsorbing onto SnO_2 surface. Previously, a quadratic dependence of absorbance on concentration confirmed the a dimeric species adsorption onto the SnO_2 surface as reported by Liu and Kamat using smaller cationic dyes, thionine, methylene blue or Ox170.[22g] The spectra in Figure 1b was further analyzed by constructing Benesi−Hildebrand plot[28] as shown in the Figure 1b inset. Here, inverse of the difference in absorbance at 449 nm was plotted against inverse of the amount of added $(TMPyP)H_2$. A linear plot

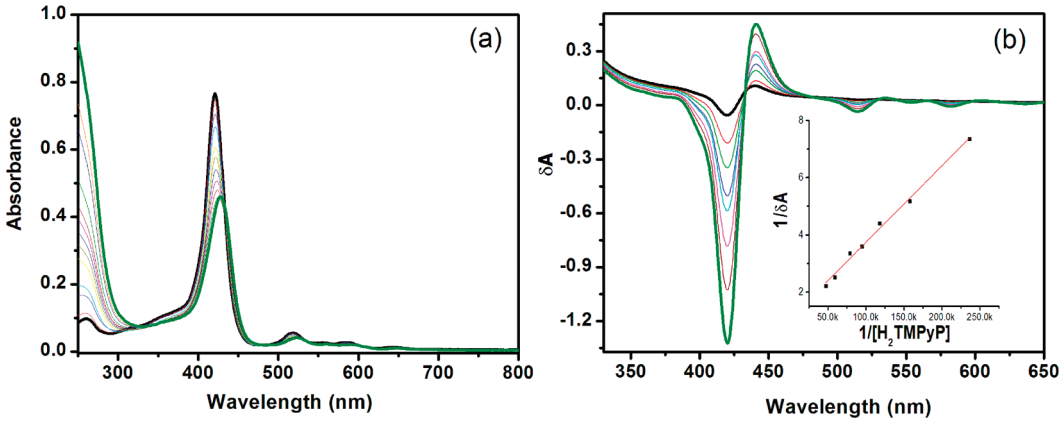

Figure 1. (a) Absorption spectral changes observed for $(TMPyP)H_2$ (3 mL of 2.17 mM) on increasing addition of colloidal SnO_2 (5−10 μL of 11.2 mM each addition) in water. (b) Absorption spectra recorded with two-beam spectrometer during addition of aqueous solution of $(TMPyP)H_2$ (5 μL of 1.4 mM each addition) to a SnO_2 (3 mL of 0.85 g/L) solution in water. $\delta A = A - A_o$, where A and A_o correspond to the absorbance of $(TMPyP)H_2$ in the presence and absence of SnO_2. Inset of b shows Benesi−Hildebrand plot showing linear dependence of the inverse δA at 449 nm on the inverse of the $(TMPyP)H_2$ concentration.

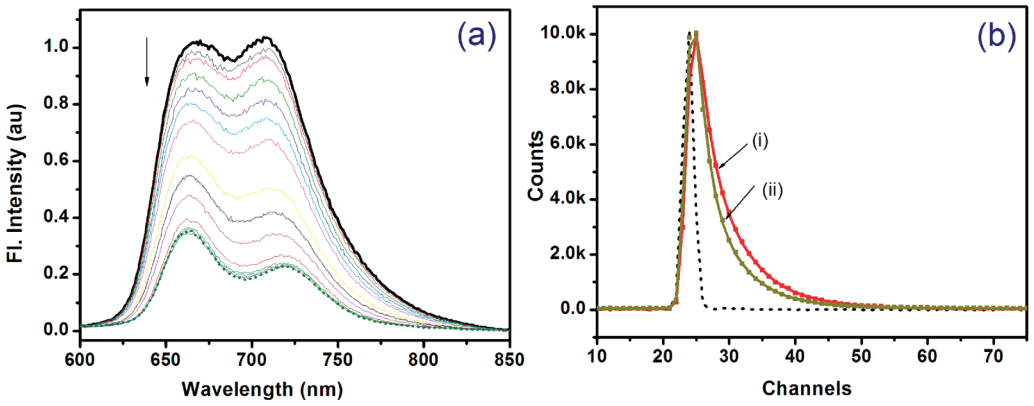

Figure 2. (a) Fluorescence spectra of $(TMPyP)H_2$ (3 mL of 2.17 μM) on increasing addition nanocrystalline SnO_2 (addition of 5−20 μL solution of 1.1 g/L concentration). λ_{ex} = 517 nm. (b) Fluorescence decay profiles of $(TMPyP)H_2$ in the absence (i) and presence (ii) of nanocrystalline SnO_2, excited at 561 nm using a nano-LED source. The lamp profile is shown in dashed line. Time calibration factor for each channel =8.77 × 10^{-10} s.

was obtained; using the slope and intercept the apparent association constant, K_a, was evaluated to be 1.5 × 10^4 M^{-1}. Similar values of K_a were obtained for rest of the water-soluble, cation porphyrins binding to SnO_2, as listed in Table 1. The K_a values found to follow the trend (TMPyP)M < (TAP)M < (TMIP)M, suggesting stronger binding of $(TMIP)H_2$, perhaps due to better geometry reasons. It may also be mentioned here that the K_a values reported here should be treated with some caution because the varying size of SnO_2 particles and aggregation of water-soluble porphyrins, especially (TMPyP)M derivatives, may restrict absolute determination of the binding constants.

Fluorescence Quenching Studies. The effect of semiconducting SnO_2 particles on the fluorescence emission of the porphyrins was investigated using both steady-state and time-resolved studies. As shown in Figure 2a for the $(TMPyP)H_2$ derivative, addition of SnO_2 quenched the fluorescence emission over 70% of its original intensity accompanied by small red shifts. This was also the case for rest of the zinc and free-base porphyrin derivatives but the percentage of quenching was generally higher for the zinc derivatives (as much as 96% in the case of (TMPyP)Zn) compared to the free-base ones (see Figures S6−S8 in the Supporting Information). To clarify whether the quenching is due to heavy atom effect, we performed control experiments involving fluorescence quenching of (TMPyP)Zn in the presence of $SnCl_2$ (see Figure S11 in the Supporting Information). The presence of $SnCl_2$ quenched the fluorescence by less than 5%, suggesting heavy atom quenching is not a likely quenching mechanism.

Further, the lifetime of free-base porphyrins were measured with incremental addition of SnO_2. The emission of both $(TAP)H_2$ and $(TMIP)H_2$ revealed monoexponential decays with lifetimes of 9.14 and 9.96 ns, respectively, when excited using a 561 nm nano-LED source. However, $(TMPyP)H_2$ revealed a biexponential decay with lifetimes of 5.2 (85%) and 1.2 (15%) ns yielding an average lifetime of 4.7 ns (Figure 2b), a result that agrees well with the literature value.[29] The decreased lifetime for TMPyP may be attributed to their strong intermolecular aggregation in solution. Addition of SnO_2 to the solution induced rapid decay and at the saturation point, the lifetimes of $(TAP)H_2$ and $(TMIP)H_2$ were found to be 2.47 and 3.51 ns, respectively, while the average lifetime of $(TMPyP)H_2$ in the presence of SnO_2 was 3.5 ns. The percent quenching by time-resolved emission were generally smaller compared to steady-state measurements indicating the presence of both static and dynamic quenching.[29] It may be mentioned here that we could not measure the lifetimes of the zinc porphyrins because of the low time resolution of the instrument.

To verify that the excited state electron transfer is the quenching mechanism, the standard free energy change for electron injection, ΔG^{o}_{inj} was estimated from the redox potentials of the donor porphyrins,[30,31] acceptor SnO_2 particles,[32] and singlet state energies of the employed porphyrins[32] according to literature methods.[33] Such data given in Table 1 and their dependence on metal ion in the porphyrin cavity clearly show that charge injection from the singlet excited porphyrin to SnO_2 is likely the quenching mechanism for all of the employed porphyrins.

By assuming the quenching is due to charge injection from the singlet excited porphyrin to conduction band of SnO_2, the rate constants were estimated according to eq 1[34]

$$k = 1/\tau_{bound} - 1/\tau_{free} \quad (1)$$

where τ_{free} and τ_{bound} represent lifetime of porphyrin in the absence of presence of SnO_2, respectively. The rates thus measured were found to be 2.95 × 10^8 s^{-1}, 1.84 × 10^8 s^{-1}, and 0.73 × 10^8 s^{-1}, respectively, for fluorescence quenching of $(TAP)H_2$, $(TMIP)H_2$, and $(TMPyP)H_2$ by SnO_2. The magnitude of k values suggest rapid charge injection and that the free-base porphyrin derivatives with peripheral positive charges away from the π-system are better candidates for charge injection, perhaps because of the slightly easier oxidation of the latter porphyrin macrocyle.[30] However, other factors may also play an important role in governing the overall efficiency as discussed in the forthcoming section.

Additional experiments were performed to visualize the stability of electrostatically adsorbed porphyrin dyes onto the SnO_2 surface by monitoring the fluorescence recovery by increasing addition of $LiClO_4$ to the solution.[35] In the case of (TAP)M, and (TMPyP)M up to 80% of the quenched porphyrin intensity could be recovered upon addition of $LiClO_4$ (Figure 3) However, for $(TMIP)H_2$ bound SnO_2 no such recovery of porphyrin emission upon addition of $LiClO_4$ was observed (see Figure S9 in the Supporting Information), suggesting much stronger binding of $(TMIP)H_2$ to the SnO_2 surface, a result that is in agreement with the calculated binding constants. This effect can also be seen visually when the (TMPyP)Zn was irradiated by UV light (Figure 3 inset). Although (TMPyP)Zn:SnO_2 resulted in a dark complex (picture c in

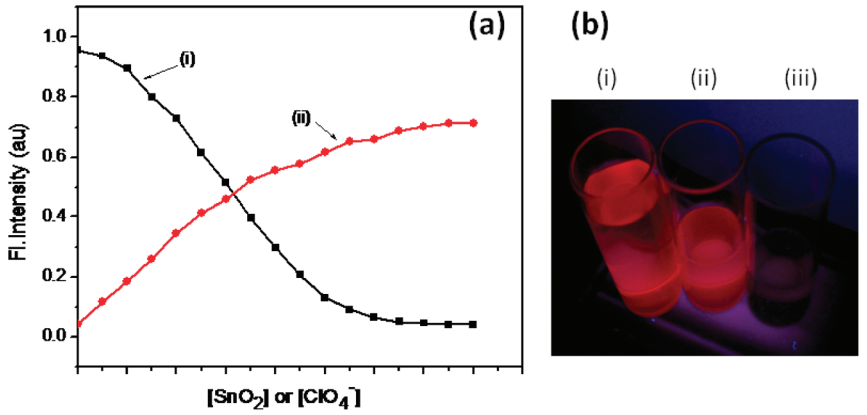

Figure 3. (a) (i) Fluorescence intensity of the 660 nm band of (TMPyP)Zn on increasing addition of nanocrystalline SnO_2 in water (each addition is 15 μL of 2.011 g/L SnO_2). (ii) Recovery of porphyrin emission on increasing addition of lithium perchlorate (each addition is 10 μL of 1.0 M solution) to a solution of (TMPyP)Zn:SnO_2 in water. (b) The picture shows fluorescence under UV irradiation of (i) (TMPyP)Zn, (ii) (TMPyP)Zn:SnO_2 in the presence of $LiClO_4$ and (iii) (TMPyP)Zn:SnO_2 complex in water.

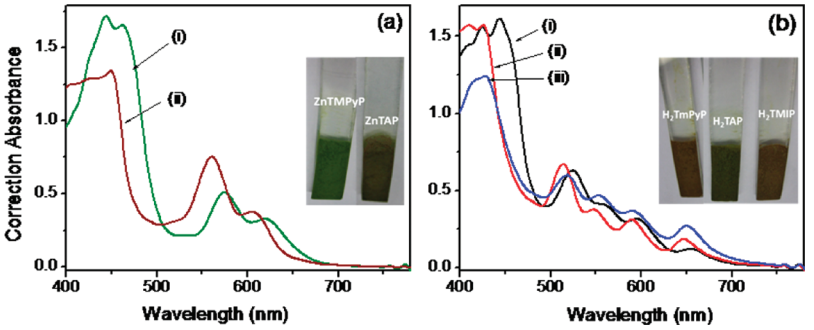

Figure 4. Corrected absorbance (background subtracted for FTO/SnO_2) spectrum of (a) zinc and (b) free-base derivatives of (i) TMPyP, (ii) TAP, and (iii) TMIP derivatives electrostatically adsorbed onto the thin film SnO_2 on FTO electrodes. The figure inset shows the picture of the respective FTO/SnO_2/(P)M electrodes.

Figure 3 inset), restoration of fluorescence upon addition of lithium perchlorate is clearly seen (picture b in Figure 3 inset), indicating the release of fluorescent porphyrin from the SnO_2 surface. It may be mentioned here that utilization of neutral porphyrin with no peripheral positive charges resulted in little or no SnO_2 surface adsorption.

Photoelectrochemical Studies. Photoelectrochemical studies were performed using SnO_2 thin-film on the FTO electrode surface after electrostatic adsorption of the positively charged porphyrins. The SnO_2 electrodes (see Experimental Section for preparation details) were dipped in ~1 mM concentration of a given porphyrin solution in methanol and the adsorption was monitored by optical absorption methods. After reaching the maximum adsorption (nearly 3 h), the electrodes were rinsed with pure methanol to remove any unbound porphyrins. They were dried at 60 °C for 10 min to remove the solvent and were used in the following studies. The amount of porphyrin on thin film SnO_2 surface for (TMPyP)Zn modified electrode, estimated from optical studies (desorption method by the addition of $LiClO_4$), was about 3.5×10^{-8} mol/cm^2. Figure 4a and b shows the absorption spectra of the adsorbed porphyrins after background subtraction for FTO/SnO_2 along with the picture of the modified electrodes. The electrodes were greenish-red, different from that of red/purple color of the porphyrins in solution indicating not a simple adsorption but a good surface interaction. High absorbance was observed in the Soret region, whereas in the visible region, the normal spectral bands corresponding to either the zinc or free-base porphyrin were apparent. It is important to note the existence of the broadened spectral bands for (TMPyP)M adsorbed electrodes suggesting occurrence of structural changes associated with flattening of the pyridyl rings to the plane of the porphyrin macrocycle upon binding to the SnO_2 surface,[27] in agreement with the absorption spectral results shown in Figure 1.

Figure 5a shows $I-V$ characteristics of the FTO/SnO_2/M(P) in the presence of I^-/I_3^- redox mediator under AM 1.5 simulated light conditions. The choice of iodide salts with regard to the cationic counterpart deserves special mention as stronger interacting cation might replace the electrostatically adsorbed porphyrins on the SnO_2 surface. After a series of trials we found that tetrabutylammonium iodide ((TBA)I) had no effect on the electrostatically adsorbed cationic porphyrins on the SnO_2 surface. This was confirmed by measuring the absorbance of the mediator I^-/I_3^- solution before and after the photoelectrochemical experiment which showed no traces of desorbed porphyrin in solution. Hence, (TBA)I was used in the preparation of the mediator I^-/I_3^- solution. As shown in Figure 5, a steady cathodic photocurrent was observed when the FTO/SnO_2/(P)M electrodes were illuminated. The short circuit current, I_{SC} ranged between 3.3 and 4.7 mA/cm^2, whereas the

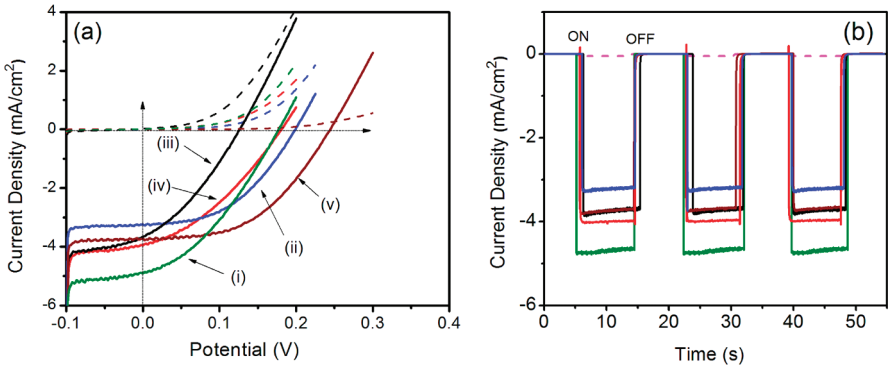

Figure 5. (a) $J-V$ plots for FTO/SnO_2/(P)M electrodes in acetonitrile containing 0.5 M (TBA)I and 0.05 M I_2 as redox mediator; (i) (TMPyP)Zn, (ii) (TAP)Zn, (iii) (TMPyP)H_2, (iv) (TAP)H_2, and (v) (TMIP)H_2 surface modified. The dotted lines show the dark currents. (b) Light on−off switching of photocurrent revealing the robustness of the electrodes. The dotted line represents currents of electrode modified with only SnO_2.

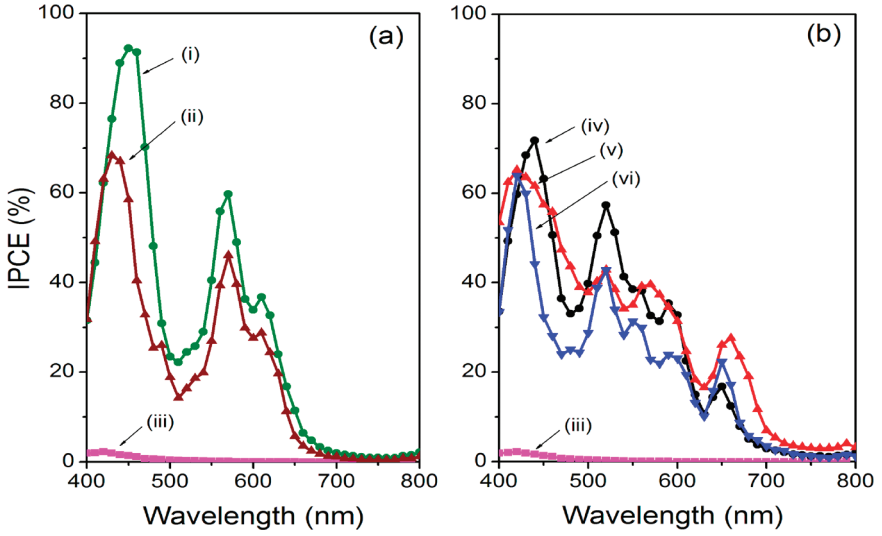

Figure 6. Incident photon-to-current conversion efficiency (IPCE) for FTO/SnO_2/(P)M electrodes in acetonitrile containing (TBA)I/I_2 (0.5 M/0.05 M) redox mediator. The porphyrins electrostatically adsorbed are: (i) (TMPyP)Zn, (ii) (TAP)Zn, (iii) no porphyrin, (iv) (TMPyP)H_2, (v) (TAP)H_2, and (vi) (TMIP)H_2, respectively, on FTO/SnO_2 surface.

open circuit potential, V_{OC}, ranged between 0.13 and 0.24 V depending on the nature of porphyrin adsorbed onto the SnO_2 surface. All of the modified electrodes revealed some dark currents beyond 0.1 V (dotted lines in Figure 5a), more so for the (TMPyP)M-modified electrodes. In the case of (TAP)M and (TMPyP)H_2, dark currents were normally lower, which was reflected in a 50−70 mV increase in V_{OC}. Such behavior was reported for SnO_2 modified with a ruthenium complex, N719,[36] and the effect was attributed to the lower conduction band edge, resulting in higher back electron transfer rates[37,38] and higher reactive trap energy states.[36] Between the free-base and zinc porphyrins, the latter revealed better performance in terms of both I_{SC} and V_{OC}, a result that could to be related to free-energy changes and bathochromic shift upon adsorption of the porphyrins. The fill-factors were also calculated from the $J-V$ plots whose values ranged between 20 and 50% with generally higher fill-factors for the zinc porphyrin derivatives. As shown in Figure 5b, the light-switching experiments revealed reproducible results, suggesting higher stability of the dye−SnO_2 of the photoelectrochemical cells.

The monochromatic incident photon-to-current conversion efficiency (IPCE), defined as the number of electrons generated by light in the outer circuit divided by the number of incident photons, was determined according to eq 2[34]

$$\mathrm{IPCE}(\%) = 100 \cdot 1240 I_{SC}(\mathrm{mAcm^{-2}})/[\lambda(\mathrm{nm}) P_{in}(\mathrm{mWcm^{-2}})] \quad (2)$$

where I_{SC} is the short-circuit photocurrent generated by the incident monochromatic light and λ is the wavelength of this light with intensity P_{in}. The photocurrent action spectrum (average of three runs) of the FTO/SnO_2/M(P)-modified electrodes in a mediator solution of 0.5 M (TBA)I and 0.05 M I_2, in acetonitrile, with a Pt foil as the counter electrode, is shown in Figure 6. The spectra resembled those of the absorption spectra shown in Figure 4a and b. At the wavelength of maximum photocurrent, the IPCE was 91% for FTO/SnO_2/(TMPyP)Zn electrode at the Soret band area for SnO_2-dye modified electrodes in a photoelectrochemical setup. Additionally, the observed red-shifted peaks of (TMPyP)M is in agreement with the optical absorption spectrum shown in Figure 4 as a consequence of flattening of the porphyrin macrocycle on the SnO_2 surface. The high IPCE values suggest that in addition to electrostatic

Table 2. Performance[a] of the FTO/SnO_2/M(P) (P = TMPyP, TAP, or TMIP) Solar Cells Investigated in the Present Work

M(P)	peak position (IPCE (%))	I_{SC} (mA/cm^2)	V_{OC} (V)	FF (%)	η (%)
(TMPyP)Zn	455(91), 570(68), 612(39)	4.7	0.18	38	0.31
(TAP)Zn	431(58), 570(45), 611(27)	3.7	0.24	50	0.45
(TMPyP)H_2	439(71), 519(57), 588(38), 590(35), 652(16)	3.7	0.13	31	0.15
(TAP)H_2	420(64), 520(43), 570(38), 590(35), 659(27)	4.0	0.18	34	0.25
(TMIP)H_2	422(63), 519(43), 556(31), 596(24), 652(22)	3.3	0.20	38	0.31

[a] See ref 40 for procedure of calculations of solar cell performance.

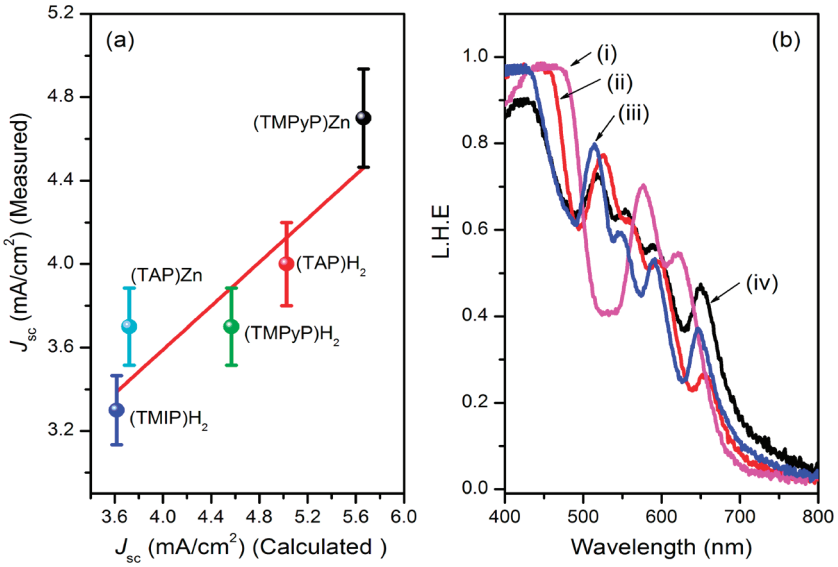

Figure 7. (a) Calculated vs measured J_{sc} for different porphyrin adsorbed electrodes. Theoretical calculation were performed using the formula $J_{sc} = \int qF(\lambda)\text{IPCE}\ (\lambda)\mathrm{d}\lambda$, where q is the electron charge and $F(\lambda)$ is the incident photon flux density for AM 1.5 standard conditions at wavelength (λ). (b) Light harvesting efficiency of (i) (TMPyP)Zn, (ii) (TMPyP)H_2, (iii) (TAP)H_2, and (iv) (TMIP)H_2 electrodes. See the Supporting Information for details of LHE calculations.

interactions, good orbital interactions between (TMPyP)M and conduction band of SnO_2 as a consequence of favorable geometry of the macrocycle (flattening of the peripheral aryl substituents to the macrocycle plane) has resulted in better charge injection.[39] Table 2 lists summary of the performance of the solar cells developed in the present study. IPCE values at each peak maxima of porphyrin are listed.

Integrating the IPCE (λ) spectrum over AM 1.5, 100 mW/cm^2 gives the theoretical current density (J_{sc}).[41] As shown in the Figure 7a, theoretical and practical values were in close agreement with a linear regression (R^2) value of 0.8 for the best fit line. Although very high IPCE values have been obtained, due to lower V_{OC}, an intrinsic property of SnO_2 and moderate fill-factors, the overall light energy conversion efficiencies were found to be relatively small, ranging between 0.15 and 0.45%.

Because IPCE is directly related to the light harvesting efficiency (LHE), the LHE for the present electrodes were also calculated using literature procedure (see the Supporting Information for details).[42] As shown in Figure 7b, for the (TMPyP)Zn-modified electrode, the efficiency was maximum (100%) in the wavelength range of 400−457 nm; however, for other electrodes, high LHE values were obtained in this range. In the Q-band range (500−700 nm range), these values were 20−80%. Such high efficiency might be attributed the very high extinction coefficient of porphyrin macrocycle in the Soret region and associated structural changes of the porphyrin macrocycle.

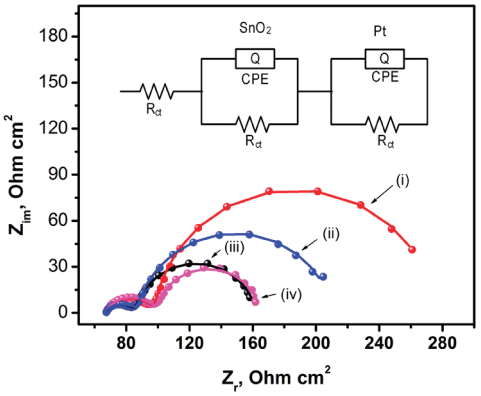

Figure 8. Impedance spectra (Nyquist plots) measured at the respective V_{OC} of (TMPyP)Zn and (TMPyP)H_2 in dark (i and ii) and under AM1.5 light conditions (iii and iv), respectively. The figure inset shows equivalent circuit diagram used to fit the data.

Electrochemical Impedance Spectroscopy (EIS) Studies. To understand the porphyrin−SnO_2/electrolyte interface, electrochemical impedance studies were performed on representative electrodes modified with (TMPyP)M (M = Zn or 2H). For photoelectrochemical cells, EIS has been a useful tool to estimate electron recombination resistance and to understand the dye

regeneration efficiency.[43] Figure 8 shows EIS results along with equivalent circuit diagram used in the analysis. Both electrodes revealed high resistance under dark conditions compared to the values under illumination. The recombination resistance under dark conditions for (TMPyP)Zn was 177.3 Ω cm^2 while that for $(TMPyP)H_2$ it was 123.0 Ω cm^2 at V_{oc}. Interestingly, under AM1.5 light conditions at V_{oc}, the recombination resistance for $(TMPyP)H_2$ was slightly higher being 76.6 Ω cm^2 than that of (TMPyP)Zn being 65.6 Ω cm^2. The decrease in the recombination resistance under light can be attributed to increased local concentration of I_3^- due to the regeneration of dye molecule by iodide near to the dye electrode interface.[43] That is, photoregeneration of (TMPyP)Zn is much efficient compared to $(TMPyP)H_2$, a result that agrees well with the cell efficiency measured by the IPCE curves in Figure 6.

Finally, a comparison between the present IPCE values with the literature results on high performance ITO/SnO_2/dye electrodes deserves special mention. Until this work, the highest IPCE for SnO_2 surface modified with a photosensitizer was for a cationic Ru(II) polypyridyl complex where a maximum IPCE of 20% at 480 nm was reported.[22d] Interestingly, for a few elegant porphyrin-fullerene donor−acceptor dyads deposited electrophoretically onto the SnO_2 surface, IPCE values up to 60% have been reported.[15−17,34,44] Clearly, the present results have demonstrated that the electrostatic binding of water-soluble cationic porphyrins to nanocrystalline SnO_2 surface under appropriate conditions of binding and electronic interactions serve as a convenient approach to obtain electrodes capable of giving near unity photon-to-electron conversion efficiencies.

4. SUMMARY

A relatively simple approach of electrostatic surface decoration of nanocrystalline thin film SnO_2 electrodes by cationic water-soluble porphyrins is demonstrated. Free-base and zinc(II) derivatives of three types of cationic water-soluble porphyrins having positive charges at distant positions of the macrocycle periphery are utilized. The porphyrin binding to SnO_2 porphyrin in water is found to be stable as revealed by their binding constants. Both steady-state and time-resolved emission spectra revealed quenching of porphyrin emission upon binding to SnO_2 in water suggesting electron injection from singlet excited porphyrin to SnO_2 conduction band. Addition of $LiClO_4$ weakened the ion-paired porphyrin-SnO_2 binding as revealed by reversible emission changes. Photoelectrochemical studies performed on FTO/SnO_2/(P)M electrodes revealed IPCE values up to 91% at the peak maxima, reported for SnO_2-dye modified electrodes. The high IPCE values have been attributed to improved charge injection due to strong electrostatic and electronic interactions between the (TMPyP)M and SnO_2, better light harvesting efficiency of porphyrins and also due to better regeneration as confirmed by EIS. Under AM 1.5 simulated light conditions, the short circuit current, I_{SC}, was on the order of 3.3−4.7 A/cm^2, and the open circuit potential, V_{OC}, was in the amount of ∼0.2 V, resulting in a maximum light conversion efficiency of 0.45%. Electrochemical impedance spectroscopy studies revealed overall decreased electron recombination resistance under light illumination conditions, more so for (TMPyP)Zn. These studies show that the decoration of cationic photosensitizers onto the SnO_2 nanoparticles under favorable electrostatic and electronic interactions is significant in terms of achieving higher photon-to-electron conversion efficiency, and this strategy can be further exploited to develop high-efficiency light energy conversion photocells.

■ ASSOCIATED CONTENT

Supporting Information. Absorption and fluorescence (steady-state and time-resolved) spectral data of cation water-soluble porphyrin binding to SnO_2. This material is available free of charge via the Internet at http://pubs.acs.org.

■ AUTHOR INFORMATION

Corresponding Author
*Corresponding Author E-mail: francis.dsouza@wichita.edu.

■ ACKNOWLEDGMENT

This work was financially supported by the National Science Foundation (Grants 0804015 and EPS-0903806) and matching support from the State of Kansas through Kansas Technology Enterprise Corporation.

■ REFERENCES

(1) O'Regan, B. C.; Grätzel, M. *Nature* **1991**, *353*, 737–740.
(2) Grätzel, M. *Inorg. Chem.* **2005**, *44*, 6841–6851.
(3) Kroon, J. M.; Bakker, N. J.; Smit, H. J. P.; Liska, P.; Thampi, K. R.; Wang, P.; Zakeeruddin, S. M.; Grätzel, M.; Hinsch, A.; Hore, S.; Wurfel, U.; Sastrawan, R.; Durrant, J. R.; Palomares, E.; Pettersson, H.; Gruszecki, T.; Walter, J.; Skupien, K.; Tulloch, G. *Prog. Photovolt. Res. Appl.* **2007**, *15*, 1.
(4) Delgado, J. L.; Bouit, P.-A.; Filippone, S.; Herranz, M. A.; Martin, N. *Chem. Commun.* **2010**, *46*, 4853–4865.
(5) Snaith, H. J.; Schmidt-Mende, L. *Adv. Mater.* **2007**, *19*, 3187–3200.
(6) Talapin, D. V.; Murray, C. B. *Science* **2005**, *310*, 86–89.
(7) Goncalves, L. M.; Zea Bermudez, V.; de Ribeiro, H. A.; Mendes, A. M. *Energy Environ. Sci.* **2008**, *1*, 655–667.
(8) Baxter, J.; Bian, Z.; Chen, G.; Dnielson, D.; Dresslhaus, M. S.; Fedorov, A. G.; Fisher, T. S.; Jones, C. W.; Maginn, E.; Kortshagen, U.; Manthiram, A.; Nozik, A.; Bolison, D. R.; Sands, T.; Shi, L.; Sholl, D.; Wu, Y. *Energy Environ, Soc.* **2009**, *2*, 559–588.
(9) (a) Martinez-Diaz, M.; de la Torre, V.; Torres, T. *Chem. Commun.* **2010**, *46*, 7090–7108. (b) Bottair, G.; de la Torre, G.; Guldi, D. M.; Torres, T. *Chem. Rev.* **2010**, *110*, 6768–6816. (c) Sgobba, V.; Guldi, D. M. *J. Mater. Chem.* **2008**, *18*, 153–157.
(10) Hamann, T. W.; Jensen, R. A.; Martinson, A. B. F.; Van Ryswyk, H.; Hupp, J. T. *Energy Environ. Sci.* **2008**, *1*, 66–78.
(11) Pagliaro, M.; Palmisano, G.; Ciriminna, R.; Loddo, V. *Energy Environ., Sci.* **2009**, *2*, 838–844.
(12) Tulloch, G. *J. Photochem. Photobiol., A* **2004**, *164*, 209–219.
(13) Moreira Goncalves, L.; de Zea Bermudez, V.; Aguilar Ribeiroa, H.; Mendes, A. M. *Energy Environ. Sci.* **2008**, *1*, 655–667.
(14) Kamat, P. V. *J. Phys. Chem. C* **2007**, *111*, 2834–2860.
(15) Umeyama, T.; Imahori, H. *Energy Environ. Sci.* **2008**, *1*, 120–133.
(16) Kamat, P. V.; Schatz, G. C. *J. Phys. Chem. C* **2009**, *113*, 15473–15475.
(17) Hasobe, T. *Phys. Chem. Chem. Phys.* **2010**, *12*, 44–57.
(18) See for example: (a) Polo, A. S.; Itokazu, M. K.; Murakami Iha, N. Y. *Coord. Chem. Rev.* **2004**, *248*, 1343–1361. (b) Abbotto, A.; Barolo, C.; Bellotto, F.; Angelis, D.; Grätzel, M.; Manfredi, N.; Marinzi, C.; Fantacci, S.; Yum, J.-H.; Nazeeruddin, M. K. *Chem. Commun.* **2008**, *42*, 5318–5320. (c) Nazeeruddin, M. K.; DeAngelis, F.; Fantacci, S.; Selloni, A.; Viscardi, G.; Liska, P.; Ito, S.; Takeru, B.; Gratzel, M. *J. Am. Chem. Soc.* **2005**, *127*, 16835–16847. (d) Nazeeruddin, M. K.; Kay, A.;

Rodicio, I.; Humphry-Baker, R.; Mueller, E.; Liska, P.; Vlachopoulos, N.; Grätzel, M. *J. Am. Chem. Soc.* **1993**, *115*, 6382–6390. (e) Chiba, Y.; Islam, A.; Watanabe, Y.; Komiya, R.; Koide, N.; Han, L. *Jpn. J. Appl. Phys.* **2006**, *2*, L638–L640. (f) Reynal, A.; Forneli, A.; Palomares, E. *Energy Environ. Sci.* **2010**, *3*, 805–812.

(19) See for example: (a) Liang, M.; Xu, W.; Cai, F.; Chen, P.; Peng, B.; Chen, J.; Li, Z. *J. Phys. Chem. C* **2007**, *111*, 4465–4472. (b) Hwang, S.; Lee, J. H.; Park, C.; Lee, H.; Kim, C.; Park; Lee, M.-H.; Lee, W.; Park, J.; Park, N.- G.; Kim, C. *Chem. Commun.* **2007**, 4887–4889. (c) Choi, H.; Baik, C.; Kang, S. O.; Ko, J.; Kang, M.-S.; Nazeeruddin, M. K.; Gratzel, M. *Angew. Chem., Int. Ed.* **2008**, *47*, 327–330. (d) Tian, H.; Yang, X.; Pan, J.; Chen, R.; Liu, M.; Zhang, Q.; Hagfeldt, A.; Sun, L. *Adv. Funct. Mater.* **2008**, *18*, 3461–3468. (e) Qin, H.; Wenger, S.; Xu, M.; Gao, F.; Jing, X.; Wang, P.; Zakeeruddin, S. M.; Zakeeruddin, G. *J. Am. Chem. Soc.* **2008**, *130*, 9202–9203. (f) Ning, Z.; Zhang, Q.; Wu, W.; Pei, H.; Liu, B.; Tian, H. *J. Org. Chem.* **2008**, *73*, 3791–3797. (g) Liu, W.-H.; Wu, I.-C.; Lai, C.-H.; Chou, P.-T.; Li, Y.-T.; Chen, C.-L.; Hsu, Y.-Y.; Chi, Y. *Chem. Commun.* **2008**, 5152–5154. (h) Ito, S.; Miura, H.; Uchida, S.; Takata, M.; Sumioka, K.; Liska, P.; Comte, P.; Pechy, P.; Grätzel, M. *Chem. Commun.* **2008**, 5194–5197. (i) Bozic-Weber, B.; Constable, E. C.; Figgemeier, E.; Housecroft, C. E.; Kylberg, W. *Energy Environ. Sci.* **2009**, *2*, 299–305. (j) Chen, K.-F.; Hsu, Y.-C.; Wu, Q.; Yeh, M.-C. P.; Sun, S.-S. *Org. Lett.* **2009**, *11*, 377–380. (k) Zhang, G.; Bala, H.; Cheng, Y.; Shi, D.; Lv, X.; Yu, Q.; Wang, P. *Chem. Commun.* **2009**, 2198–2200. (l) Li, G.; Zhou, Y.-F.; Cao, X.-B.; Bao, P.; Jiang, K.-J.; Lin, Y.; Yang, L.-M. *Chem. Commun.* **2009**, 2201–2203. (m) Li, R.; Lv, X.; Shi, D.; Zhou, D.; Cheng, Y.; Zhang, G.; Wang, P. *J. Phys. Chem. C* **2009**, *113*, 7469–7479. (n) Mishra, A.; Fischer, M. K. R.; Bauerle, P. *Angew Chem., Int. Ed.* **2009**, *48*, 2474–2499.

(20) See for example: (a) Hagberg, D. P.; Edvinsson, T.; Marinado, T.; Boschloo, G.; Hagfeldt, A.; Sun, L. *Chem. Commun.* **2006**, 2245–2247. (b) Justin Thomas, K. R.; Hsu, Y.-C.; Lin, J. T.; Lee, K.-M.; Ho, K.-C.; Lai, C.-H.; Cheng, Y.- M.; Chou, P.-T. *Chem. Mater.* **2008**, *20*, 1830–1840. (c) Hagberg, D. P.; Yum, J.-H.; Lee, H.; De Angelis, F.; Marinado, T.; Karlsson, K. M.; Humphry-Baker, R.; Sun, L.; Hagfeldt, A.; Grätzel, M.; Nazeeruddin, M. K. *J. Am. Chem. Soc.* **2008**, *130*, 6259–6266. (d) Erten-Ela, S.; Yilmaz, M. D.; Icli, B.; Dede, Y.; Icli, S.; Akkaya, E. U. *Org. Lett.* **2008**, *10*, 3299–3302. (e) Radivojevic, I.; Varoto, A.; Farley, C.; Drain, C. M. *Energy Environ. Sci.* **2010**, *3*, 1897–1909.

(21) See for example:Kalyanasundaram, K.; Grätzel, M. *Coord. Chem. Rev.* **1998**, *177*, 347–414. (b) Deb, S. *Sol. Energy Mater. Sol. Cells* **2005**, *88*, 1–10. (c) Sayama, K.; Sugihara, H.; Arakawa, H. *Chem. Mater.* **1998**, *10*, 3825–3832. (d) Kitiyanan, A.; Yoshikawa, S. *Mater. Lett.* **2005**, *59*, 4038–4040. (e) Tennakone, K.; Kumara, G.; Kottegoda, I.; Perera, V. *Chem. Commun.* **1999**, 15–16. (f) Huang, M.; Mao, S.; Feick, H.; Yan, H.; Wu, Y.; Kind, H.; Weber, E.; Russo, R.; Yang, P. *Science* **2001**, *292*, 1897–1899.

(22) (a) Miyasaka, T.; Watanabe, T.; Fujishima, A.; Honda, K. *J. Am. Chem. Soc.* **1978**, *100*, 6657–6665. (b) Kamat, P. V.; Fox, M. A.; Fatiadi, A. *J. Am. Chem. Soc.* **1984**, *106*, 1191–1197. (c) Krishnan, M.; Zhang, X.; Bard, A. J. *J. Am. Chem. Soc.* **1984**, *106*, 7371. (d) Bedja, I.; Hotchandani, S.; Kamat, P. V. *J. Phys. Chem.* **1994**, *98*, 4133–4139. (e) Bedja, I.; Hotchandani, S.; Carpentieer, R.; Fessenden, R.; Kamat, P. V. *J. Appl. Phys.* **1994**, *75*, 5444–5447. (f) Kim, Y.-S.; Liang, K.; Law, K.-Y.; Whitten, D. G. *J. Phys. Chem.* **1994**, *98*, 984–988. (g) Liu, D.; Kamat, P. V. *J. Electrochem. Soc.* **1995**, *142*, 835–839. (h) Dang, X.; Hupp, J. T. *J. Photochem. Photobiol., A: Chem.* **2001**, *143*, 251–256.

(23) Kay, A.; Grätzel, M. *Chem. Mater.* **2002**, *14*, 2930–2935.

(24) (a) Ito, S.; Makari, Y.; Kitamura, T.; Wada, Y.; Yanagida, S. *J. Mater. Chem.* **2004**, *14*, 385–390. (b) Senevirathna, M. K. I.; Pitigala, P.; Premalal, E. V. A.; Tennakone, K.; Kumara, G. R. A.; Konno, A. *Sol. Energy Mater. Sol. Cells* **2007**, *91*, 544–547. (c) Snaith, H. J.; Ducati, C. *Nano Lett.* **2010**, *10*, 1259–1265.

(25) See for example: Subbaiyan, N. K.; Wijesinghe, C. A.; D'Souza, F. *J. Am. Chem. Soc.* **2009**, *131*, 14646–14647.

(26) (a) Hambright, P.; Fleischer, E. B. *Inorg. Chem.* **1970**, *9*, 1757–1761. (b) Pasternack, R. F.; Francesconi, L.; Raff, D.; Spiro, E. *Inorg. Chem.* **1973**, *12*, 2606–2611.

(27) Chernia, Z.; Gill, D. *Langmuir* **1999**, *15*, 1625–1633.

(28) Benesi, H. A.; Hildebrand, J. H. *J. Am. Chem. Soc.* **1949**, *71*, 2703–2707.

(29) Lakowicz, J. R. *Principles of Fluorescence Spectroscopy*, 3rd ed.; Springer: Singapore, 2001.

(30) Kalyanasundaram, K.; Neumann-Spaliart, M. *J. Phys. Chem.* **1982**, *86*, 5163–5169.

(31) Kadish, K. M.; Caemelbecke, E. V.; Royal, G. In *The Porphyrin Handbook*; Kadish, K. M., Smith, K. M., Guilard, R., Eds.; Academic Press: New York, 2000; Vol. 8, Chapter 55.

(32) Heyrovsky, M.; Mirkovsky, J. *Langmuir* **1995**, *11*, 4293–4299.

(33) Ford, W. E.; Rodgers, M. A. J. *J. Phys. Chem.* **1994**, *98*, 3822–3831.

(34) Hasobe, T.; Saito, K.; Kamat, P. V.; Troiani, V.; Qui, H.; Solladie, N.; Kim, K. S.; Park, J. K.; Kim, D.; D'Souza, F.; Fukuzumi, S. *J. Mater. Chem.* **2007**, *17*, 4160–4170.

(35) Seery, M. K.; Guerin, L.; Forster, R. J.; Gicquel, E.; Hultgren, V.; Bond, A. M.; Wedd, A. G.; Keyes, T. K. *J. Phys. Chem. A* **2004**, *108*, 7399–7405.

(36) (a) Prasittichai, C.; Hupp, J. T. *J Phys Chem Lett.* **2010**, *1*, 1611–1615. (b) Ito, S.; Liska, V.; Comte, P.; Charvet, R. L.; Pechy, P.; Bach, U.; Schmidt-Mende, L.; Zakeeruddin, S. M.; Kay, A.; Nazeeruddin, M. K.; Gratzel, M. *Chem. Commun.* **2005**, 4351–4353. (c) Liu, D.; Fessenden, R. W.; Hug, G. L.; Kamat, P. V. *J. Phys. Chem. B* **1997**, *101*, 2583–2590.

(37) Gubbala, S.; Russell, H. B.; Shah, H.; Deb, B.; Jasinski, J.; Rypkema, H.; Sunkara, M. K. *Energy Environ. Sci.* **2009**, *2*, 1302–1309.

(38) Green, A. N. M.; Palomares, E.; Haque, S. A.; Kroon, J. M.; Durrant, J. R. *J. Phys. Chem. B* **2005**, *109*, 12525–12533.

(39) Halme, J.; Vahermaa, P.; Miettunen, K.; Lund, P. *Adv. Mater.* **2010**, *22*, E210–E234.

(40) Kelly, J. J.; Hens, Z.; Vanmaekelbergh, D.; Hensalso, Z. L.M. In *Encyclopedia of Electrochemistry*; Bard, A. J., Stratmann, M., Eds.; Wiley—VCH: Weinheim, Germany, 2003; Vol. 6, pp 59—105.

(41) Guo, X.-Z.; Luo, Y.-H.; Li, C.-H.; Qin, D.; Li, D.-M.; Meng, Q.-B. *Curr. Appl. Phys.* **2011**No. DOI: 10.1016/j.cap.2011.03.060.

(42) Hagfeldt, A.; Peter, L In *Dye-Sensitized Solar Cells*; Kalyanasundaram, K., Ed.; EPFL Press: Lausanne, Switzerland, 2010; Chapter 10, pp 324—402.

(43) (a) Wang, Q.; Moser, J.-E.; Gratzel, M. J. *Phys. Chem. B* **2005**, *109*, 14945–14953.(b) Bisquert, J.; Fabregat-Santiago, F. In *Dye-Sensitized Solar Cells*; Kalyanasundaram, K., Ed.; EPFL Press: Lausanne, Switzerland, 2010; Chapter 12, pp 457—554.

(44) (a) Fungo, F.; Otero, L.; Durantini, E. N.; Silber, J. J.; Sereno, L. E. *J. Phys. Chem. B* **2000**, *104*, 7644–7651. (b) Imahori, H.; Liu, J.-C.; Hotta, H.; Kira, A.; Umeyama, T.; Matano, Y.; Li, G.; Ye, S.; Isosomppi, M.; Tkachenko, N. V.; Lemmetyinen, H. *J. Phys. Chem. B* **2005**, *109*, 18465–18474. (c) Imahori, H.; Ueda, M.; Kang, S.; Hayashi, H.; Hayashi, S.; Kaji, H.; Seki, S.; Saeki, A.; Tagawa, S.; Umeyama, T.; Matano, Y.; Yoshida, K.; Isoda, S.; Shiro, M.; Tkachenko, N. V.; Lemmetyinen, H. *Chem.—Eur. J.* **2007**, *12*, 10182–10193. (d) Umeyama, T.; Tezuka, N.; Seki, S.; Matano, Y.; Nishi, M.; Hirao, K.; Lehtivuori, H.; Tkachenko, N. V.; Lemmetyinen, H.; Nakao, Y.; Sakaki, S.; Imahori, H. *Adv. Mater.* **2010**, *22*, 1–4.